Output temporal contrast simulation of a large aperture high power short pulse laser system

Ping Zhu[1,2], Xinglong Xie[1], Xiaoping Ouyang[1], and Jianqiang Zhu[1]

[1]*Joint Laboratory on High Power Laser and Physics, Shanghai Institute of Optics and Fine Mechanics, Chinese Academy of Sciences, Shanghai, China*

[2]*University of Chinese Academy of Sciences, Beijing, China*

Abstract

The work presented in this paper is a study of output temporal contrast degradation by near-field quality deterioration, such as intensity modulation and wavefront deviation, in a large aperture high power short pulse laser system. A two-step focusing algorithm with a coordinate transform based on the Fresnel approximation in the space domain is used for simulating the output focused by an off-axis parabolic mirror. The temporal contrast degradation by intensity modulation and wavefront deviation is analyzed and the influence of the diameter on the temporal contrast degradation is revealed. The simulation and assumption results based on the parameters of the Shen Guang-II laser system are compared with the online experimental temporal contrast data. The near-field quality deterioration might lead to temporal contrast degradation, hindering higher temporal contrast in large aperture high power short pulse laser systems.

Keywords: fill factor of laser beam; temporal contrast; ultrafast optics; wavefront deviation

1. Introduction

With the development of chirped-pulse amplification (CPA) and optical parametric CPA (OPCPA), extremely intense short pulse laser systems are increasingly applied to experimental investigations in 'fast ignition' inertial confinement fusion (ICF), laser–plasma interactions and strong field physics[1]. The European Extreme Light Infrastructure (ELI) has designed a 25 PW, 10^{25} W cm^{-2} single laser beamline (ILE)[2], in which the high temporal contrast required by pre-plasma-free interactions[3] will be one of the major challenges. Various factors resulting in temporal contrast degradation have been analyzed and verified, such as gain saturation[4], asymmetric spectral clipping[5], self-phase modulation [6], amplified spontaneous emission (ASE) in the CPA system[7] and pump distortion-induced noise (PDN)[8], surface-reflection-initiated pre-pulses[9] and parametric fluorescence (PF)[10] in the OPCPA system, etc.

High energy laser systems usually enlarge the beam diameter to reduce the energy density on optical elements to mitigate the limited damage threshold problem, which inevitably leads to worse near-field quality, such as near-field intensity modulation and wavefront deviation. Means have existed for some time to analyze the influence on spatial output characteristics by wavefront deviation[11]. However, the discussed temporal characteristics in the wavefront deviation situation only cover the pulse width[12], leaving the temporal contrast degradation by intensity modulation and wavefront deviation unclear.

In large aperture high power short pulse laser systems, the output is focused by an off-axis parabolic mirror (OAP), and this focusing propagation can be well simulated by a two-step coordinate transformed focusing method, not only taking advantage of using coordinate transformation but also avoiding the contradiction between the space scale and the diffraction limit[13]. Using this method, this paper simulates the output temporal contrast of a large aperture high power short pulse laser system. The temporal contrast degradation by intensity modulation and wavefront deviation is analyzed, the influence of the diameter on the temporal contrast degradation is revealed and the simulation and assumption results based on the parameters of the Shen Guang-II (SG-II) laser system are compared with the online experimental temporal contrast data. The conclusion can be drawn that the near-field quality is one of the possible factors hindering higher temporal contrast in large aperture high power short pulse laser systems.

Correspondence to: P. Zhu, Shanghai Institute of Optics and Fine Mechanics, Chinese Academy of Sciences, No. 390, Qinghe Road, Jiading District, Shanghai 201800, China. Email: zhp1990@siom.ac.cn

1

2. Theory and simulation

2.1. Model

In practical short pulse applications, the amplified pulse by CPA or OPCPA will be focused onto the target using an OAP after being compressed by a grating compressor. The analogy can be made between the OAP focusing subsystem and an ideal lens, because it linearly reflects propagation in free space without dispersion, chromatic aberration or B-integral nonlinear effects, the spatial intensity distribution of which can be calculated by the Fresnel diffraction integral formula:

$$
\begin{aligned}
&U(x, y, L, \omega) \\
&= \frac{\exp(\mathrm{i}kL)}{\mathrm{i}\lambda L} \iint_{-\infty}^{\infty} U_0(x_0, y_0, 0) \exp\left(-\mathrm{i}k\frac{x^2 + y^2}{2f}\right) \\
&\quad \times \exp\left\{\frac{\mathrm{i}k}{2L}[(x - x_0)^2 + (y - y_0)^2]\right\} dx_0 dy_0, \quad (1)
\end{aligned}
$$

where x and y are the coordinates in the observation plane $(z = L)$, x_0 and y_0 are the coordinates in the incident plane, $\lambda = 2\pi c/\omega$ is the wavelength of the incident pulse, $k = 2\pi/\lambda$ is the wavevector and f is the focal length of the OAP.

For higher spatial resolution and a more accurate result, on applying the coordinate transforms $x' = x/(1 - L/f)$, $y' = y/(1 - L/f)$ and $z' = z/(1 - L/f)$, Equation (1) becomes

$$
\begin{aligned}
&U'\left(x', y', \frac{fL}{f-L}\right) \\
&= \frac{\exp\left(\mathrm{i}k\frac{fL}{f-L}\right)}{\mathrm{i}\lambda \frac{fL}{f-L}} \iint_{-\infty}^{\infty} U_0(x_0, y_0, 0) \\
&\quad \times \exp\left\{\frac{\mathrm{i}k}{2\frac{fL}{f-L}}[(x' - x_0)^2 + (y' - y_0)^2]\right\} dx_0 dy_0 \\
&= F_{\mathrm{space}}^{-1}\left\{H\left(f_X, f_Y, \frac{fL}{f-L}\right) \cdot F_{\mathrm{space}}[U_0(x_0, y_0, 0)]\right\},
\end{aligned}
$$
$$(2)$$

$$
\begin{aligned}
H(f_X, f_Y, z) &= \exp(\mathrm{i}kz) \exp[-\mathrm{i}\pi\lambda z(f_X^2 + f_Y^2)] \\
&\quad \text{(Fresnel diffraction)}, \\
&= \exp\left[\mathrm{i}2\pi\frac{z}{\lambda}\sqrt{1 - (\lambda f_X)^2 - (\lambda f_Y)^2}\right] \\
&\quad \text{(angular spectrum diffraction)}. \quad (3)
\end{aligned}
$$

Here, $f_X = x/\lambda z$ and $f_Y = y/\lambda z$ are the spatial frequencies in the x and y directions, respectively, and the spatial Fourier transform and its inverse form are introduced to reduce the computing time by the fast Fourier transform (FFT) algorithm:

$$
F_{\mathrm{space}}(u) = \iint u(x, y) \exp[-\mathrm{i}2\pi(f_X x + f_Y y)]dxdy,
$$

$$
F_{\mathrm{space}}^{-1}(U) = \iint U(f_X, f_Y) \exp[\mathrm{i}2\pi(f_X x + f_Y y)]df_X df_Y.
$$
$$(4)$$

When Equation (2) is applied to focusing propagation $(L = f)$, a problem of infinite x', y' and z' is encountered, which can be ingeniously resolved by a two-step simulation, first calculating from $z = 0$ to $z = L$ with coordinate transforms and finally calculating from $z = L$ to $z = f$ without coordinate transforms, in which angular spectrum diffraction theory is applied. The value of L is related to the coordinate magnification, which determines whether there are sufficient effective sampling points in the focal spot area. At the same time, the value of L determines whether the situation meets the requirement for the Fresnel approximation in step one with coordinate transforms. With this method in two spatial dimensions, the calculation of the focusing characteristics of a short wavelength laser beam through a short focus system has been successfully made[13].

Thus, we can use an operator P_{space} to represent the above focusing calculation:

$$
U(x, y, z, \omega) = P_{\mathrm{space}}[U(x, y, 0, \omega)]. \quad (5)
$$

The output field as a function of time is given by the inverse time Fourier transform:

$$
\begin{aligned}
U(x, y, z, t) &= F_{\mathrm{time}}^{-1}[U(x, y, z, \omega)] \\
&= \int_{-\infty}^{\infty} P_{\mathrm{space}}[U(x, y, 0, \omega)] \exp(\mathrm{i}\omega t)d\omega. \quad (6)
\end{aligned}
$$

Then, the temporal contrast can be derived by the temporal distribution of the normalized pulse intensity. In this paper, simulation of one dimension in space is used to demonstrate the influence of spatial near-field quality on temporal contrast. The idea of the two-step coordinate transformed space–time propagation simulation is shown in Figure 1.

2.2. Near-field intensity modulation

In large aperture high power laser systems, light beams are always shaped into flattened Gaussian beams (FGBs) for higher energy extraction efficiency and slower nonlinear growth. A FGB of order N and spot size ω_0 has the following normalized field distribution[14]:

$$
I_N(r) = \exp\left[-\frac{(N+1)r^2}{\omega_0^2}\right] \sum_{n=0}^{N} \frac{1}{n!}\left(\frac{\sqrt{N+1}r}{\omega_0}\right)^{2n}, \quad (7)
$$

where r is the radial coordinate.

In practical applications, the real near-field intensity is always modulated rather than an ideal FGB due to multiple causes, such as diffraction and nonlinear growth. The fill factor (FF) of the laser beam is usually used to describe
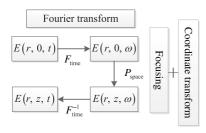
Figure 1. The simulation algorithm of time and space focusing.

the uniformity of the modulated near-field intensity, which is defined as the ratio of the average intensity and the peak intensity in the flattened area:

$$\text{FF} = I_{\text{avg}}/I_{\text{max}}. \qquad (8)$$

2.3. Wavefront deviation

The ideal incident wavefront is plane; however, it can be easily deviated by phase shifts from the optical system and optical elements. Phase shifts from the optical system, such as thermal deformation and inhomogeneity of the medium, mainly contribute to dynamic wavefront deviation on a large spatial scale, which can be detected online by a Shack–Hartmann wavefront sensor. According to research carried out at Lawrence Livermore National Laboratory[15, 16], the phase shifts from optical elements, as the main component of static wavefront deviation, can be divided into three spatial frequency regions: figure (0–0.03 mm^{-1}), waviness (0.03–8 mm^{-1}) and roughness (higher than 8 mm^{-1}), which can be expressed by the improved noise model[17]:

$$\phi(x,\,y) = \sum C_i \cdot R_i(-1,1) * \exp\left\{-\left[\left(\frac{x}{s_{ix}}\right)^2 + \left(\frac{y}{s_{iy}}\right)^2\right]\right\}, \qquad (9)$$

where C_i is the noise magnitude, $R_i(-1, 1)$ is a random function distributed between -1 and 1, $*$ represents a convolution operation, s_{ix} and s_{iy} are the spatial scales in the x and y directions, respectively, determining the noise spatial length. The total wavefront deviation is the sum of noise of every spatial length. Common evaluation indices of wavefront deviation are the peak to valley (PV) value, root mean square (RMS), RMS gradient (GRMS) and power spectral density (PSD) curve.

3. Results and discussion

The parameters of the analyzed large aperture high power short pulse model are those of the SG-II laser system[18]. A short pulse of 290 mm near-field diameter (ninth-order FGB) and 5 ps pulse width (Gaussian) at a center wavelength of 1053 nm is focused by an OAP of 800 mm focal length

and 320 mm diameter. The two-step coordinate transformed focusing method is used, while the computer samples 2048 points in space from -160 to 160 mm and 2048 points in time from -100 to 100 ps. The value of L is the key parameter of the simulation due to the two reasons mentioned above. Here, we use $L = 0.9997f$–$0.9999f$ to reach the requirements of both high resolution and the Fresnel approximation, then we obtain the convergence results.

3.1. Temporal contrast degradation by intensity modulation

First, the influence of intensity modulation on temporal contrast is analyzed. The model applied here is a ninth-order FGB with a diameter of 290 mm, and its near-field intensity is modulated randomly in three situations for which the FFs are 0.4, 0.6 and 0.8, respectively, as shown in Figure 2(a). The temporal profile of the incident pulse is Gaussian type with a pulse width (FWHM) of 5 ps. No wavefront deviation is introduced during the focusing propagation.

Figure 2(b) shows the temporal contrast degradation by intensity modulation with different FFs. If there is no intensity modulation, the temporal contrast is better than 10^9 (blue dashed line). A pre-pulse can be seen 50 ps before the main pulse when the near-field intensity is modulated, which leads to a poor temporal contrast. Moreover, the front edge of the main pulse becomes moderate 10–20 ps ahead of the peak point, which means that the pulse width of the main pulse will be broadened at the same time. When the intensity is modulated by a FF of 0.6, the temporal contrast will be degraded by more than one order of magnitude to worse than 10^8 in the time window of 50 ps before the main pulse. The tendency can be seen from this figure that the smaller the FF of the modulated intensity is the worse the output temporal contrast is.

3.2. Temporal contrast degradation by wavefront deviation

Second, using the same model as described above, the effect of wavefront deviation on temporal contrast is discussed. At this time the incident intensity has no modulation, but various types of random wavefront deviations are introduced in the focusing propagation, which have different magnitudes and different spatial frequencies. As shown in Figure 3(a), these four wavefront deviations are illustrated in the form of PSD curves.

Figure 3(b) shows the temporal contrast degradation by different types of wavefront deviations. If there is no wavefront deviation, the temporal contrast will be better than 10^9. Comparing the blue line (PV $= 0.5\lambda$) with the green line (PV $= 0.1\lambda$) in the same spatial frequency range (the same minimum spatial period T is 40 mm, which means that the same maximum spatial frequency is 0.025 mm^{-1}), the wavefront deviation with larger PV value will cause
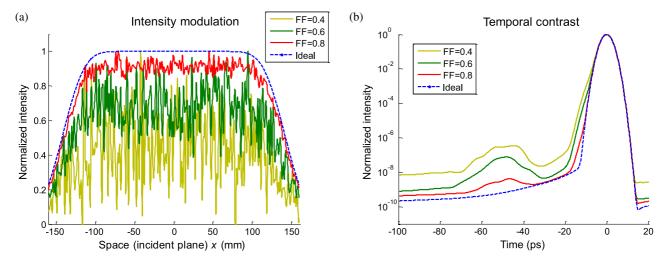
Figure 2. Temporal contrast degradation by intensity modulation. (a) Intensity modulation for different FFs (0.4, 0.6 and 0.8). (b) Temporal contrast for the different intensity modulations. The dashed line is the ideal situation without modulation.
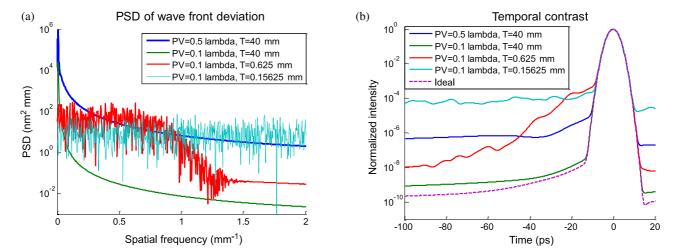

Figure 3. Temporal contrast degradation by wavefront deviation. (a) PSDs of wavefront deviations of different magnitudes and spatial frequencies. (b) Temporal contrasts for different wavefront deviations.

more severe temporal contrast degradation and in this spatial frequency range the temporal contrast will be two orders of magnitude worse than that of the ideal situation.

When the wavefront deviations have the same magnitude (PV = 0.1λ) but different spatial frequency ranges, as shown in Figure 3(b), there are large differences between the temporal contrast degradations. The wavefront deviation with the highest maximum spatial frequency of 6.4 mm^{-1} (cyan line; minimum spatial period of 0.15625 mm) causes huge degradation of more than five orders of magnitude from 10^9 to 10^4, while the wavefront deviation with the lowest maximum spatial frequency of 0.025 mm^{-1} (green line; minimum spatial period of 40 mm) induces smaller degradation of one order. Interestingly, temporal contrast degradation by the wavefront deviation with the middle maximum spatial frequency of 1.6 mm^{-1} (red line; minimum spatial period of 0.625 mm) is quite notable within 40 ps before the main

pulse; however, it becomes less significant beyond 40 ps before the main pulse. Therefore, higher spatial frequency contributes to temporal contrast degradation in a larger time window and for the same magnitude the wavefront deviation with low maximum spatial frequency has a slight influence on temporal contrast.

3.3. Influence of diameter on temporal contrast degradation

Third, the importance of discussing temporal contrast in a system with large diameter is demonstrated by analyzing the influence of diameter on temporal contrast degradation. In this case, introducing the same magnitude and same spatial frequency wavefront deviation as shown in Figures 4(a) and (b), we consider three models with different diameters: 320 (blue solid line), 160 (green solid line) and 80 mm (red solid line). The focal length is fixed at 800 mm.
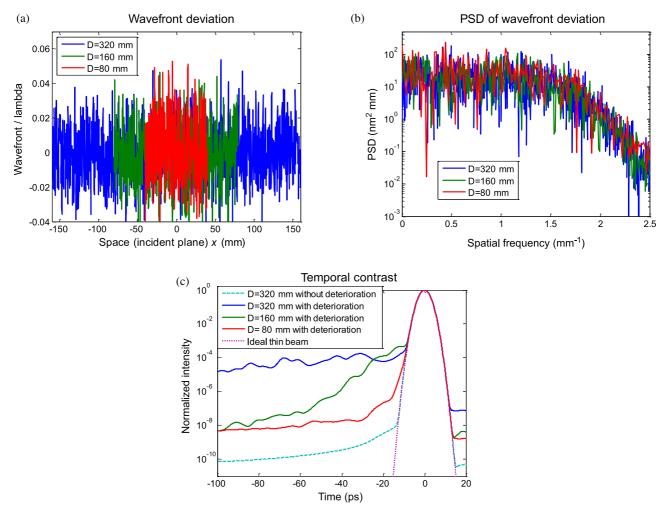
Figure 4. Influence of diameter on temporal contrast degradation. (a) Wavefront deviations for different diameters. (b) PSDs of wavefront deviations for different diameters. (c) Temporal contrasts for different diameters.

The result can be seen in Figure 4(c). The temporal contrast for 80 mm diameter is three orders of magnitude better than that for 320 mm diameter and the model with larger diameter suffers more severe temporal contrast degradation. The temporal contrast is around 10^{10} in the model with 320 mm diameter without any near-field quality deterioration (cyan dashed line). However, for an ideal thin beam that does not need to be focused, the temporal contrast will be promoted to the computer simulation resolution limit, about 10^{30} (purple dotted line). Therefore, temporal contrast degradation deserves more attention in larger aperture high power short pulse laser systems.

3.4. Simulation of temporal contrast degradation compared with experimental measurement results

Finally, the simulation model is combined with the near-field quality measured in the established SG-II large aperture high power short pulse laser system. Figure 5(a) shows the experimental near-field intensity detected in the incident plane

and Figure 5(b) shows the experimental intensity modulation (green solid line) and ideal spatial profile (blue dashed line) in one dimension. The calculated FF for the experimental near-field intensity modulation is 0.73. Figure 5(c) shows the experimental dynamic wavefront deviation detected online by a Shack–Hartmann wavefront sensor, which is unable to show waviness or roughness in the intermediate and higher frequency regions. Thus, in this case, no waviness and roughness are introduced into the simulation model. The experimental dynamic wavefront deviation in one dimension and its PSD curve are illustrated as the violet lines in Figures 5(d) and (e). After the propagation through the OAP focusing subsystem, the output temporal contrast can be obtained. In Figure 5(f), the cyan dashed line is the ideal output temporal contrast; the red solid line is the online experimental measurement result and the blue solid line is the calculation result. The online experimental measurement result[19] shows a degraded temporal contrast of 10^4, while the calculation result shows a temporal contrast degradation of less than two orders of magnitude from 10^9. There are two

(a) Experimental near field intensity

(b) Intensity modulation

(c) Experimental dynamic wave front deviation

(d) Wave front deviation

PV=2.5214 lambda
RMS=0.51218 lambda
GRMS=3.7104 lambda/cm

(e) PSD of wave front deviation
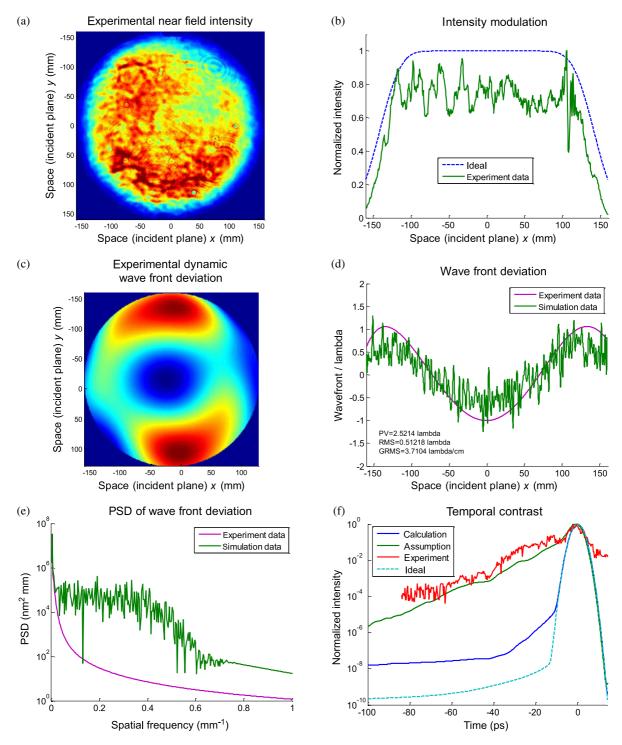
(f) Temporal contrast

Figure 5. Experimental and simulated intensity modulation, wavefront deviation and temporal contrast degradation. (a) Experimental near-field intensity. (b) Intensity modulation. (c) Experimental dynamic wavefront deviation. (d) Wavefront deviation. (e) PSD of wavefront deviation. (f) Temporal contrast.

reasons why the two results differ. (1) In this model beam quality is considered as the only influencing factor; however, in real experiments there are many other characteristics, such as ASE, PF and spectral modulation. (2) Only near-field intensity and low spatial frequency wavefront deviation are introduced, without considering waviness and roughness.

To introduce the waviness and roughness into the simulation model, an assumption is made based on the SG-II short pulse laser system configuration. In consideration of the cutoff frequency of the spatial filter, a wavefront deviation of waviness and roughness whose maximum spatial frequency is 0.6 mm^{-1} is added, as shown in Figure 5(d) by the

green line. The PV of total wavefront deviation is 2.5λ, the RMS is 0.5λ, the GRMS is $3.7\lambda\,\mathrm{cm}^{-1}$ and the PSD curve is shown in Figure 5(e) by the green line. These values are gradually adjusted since there are no online measurement data for the system. After considering the waviness and roughness, there is serious temporal contrast degradation of more than three orders of magnitude from the temporal contrast degradation level due to only intensity modulation and low spatial frequency wavefront deviation. In addition, the assumption result has a similar trend to the online experimental measurement result, in spite of the discrepancy due to some other factors. From this point of view, high spatial frequency wavefront deviations, such as waviness and roughness, influence the temporal contrast more seriously; therefore, waviness and roughness deserve careful attention, and methods of measurement and control of the wavefront deviation within the abovementioned spatial frequency region should be investigated further.

4. Conclusion

In this paper, a two-step coordinate transformed focusing method is used to simulate the output focused by an OAP in a large aperture high power short pulse laser system, and thus the output temporal contrast is calculated. The temporal contrast degradation by intensity modulation and wavefront deviation is analyzed. It is found that intensity modulation with a smaller FF and larger wavefront deviation causes more severe temporal contrast degradation, and this degradation is closely related to the spatial frequency of the total wavefront deviation. Then, the importance of discussing temporal contrast in a system with large diameter is demonstrated by analyzing the influence of diameter on temporal contrast degradation. Finally, with experimental intensity modulation, experimental low spatial frequency wavefront deviation and assumed higher spatial frequency wavefront deviation using the parameters of the SG-II laser system, the output temporal contrast is derived, which shows that waviness and roughness influence the temporal contrast more seriously. Therefore, the conclusion can be drawn that near-field quality deterioration might lead to temporal contrast degradation, hindering higher temporal contrast in large aperture high power short pulse laser systems.

Due to the lack of effective tools to measure intermediate and higher spatial frequency wavefront deviation, the need for online monitoring of the wavefront deviation in these frequency regions in large aperture high power short pulse laser systems is put forward. Improvement of the laser near-field quality might be a new method towards high temporal contrast in large aperture high power short pulse laser systems.

References

1. H. Kiriyama, T. Shimomura, M. Mori, Y. Nakai, M. Tanoue, S. Kondo, S. Kanazawa, A. S. Pirozhkov, T. Z. Esirkepov, Y. Hayashi, K. Ogura, H. Kotaki, M. Suzuki, I. Daito, H. Okada, A. Kosuge, Y. Fukuda, M. Nishiuchi, M. Kando, S. V. Bulanov, K. Nagashima, M. Yamagiwa, K. Kondo, A. Sugiyama, P. R. Bolton, S. Matsuoka, and H. Kan, Appl. Sci. **3**, 214 (2013).
2. J.-P. Chambaret, F. Canova, R. L. Martens, G. Cheriaux, G. Mourou, A. Cotel, C. Le Blanc, F. Druon, P. Georges, N. Forget, F. Ple, and M. Pittman, in *Proceedings of CLEO/Quantum Electronics and Laser Science Conference and Photonic Applications Systems Technologies* JWC4 (2007).
3. M. Kaluza, J. Schreiber, M. I. K. Santala, G. D. Tsakiris, K. Eidmann, J. Meyer-ter-Vehn, and K. J. Witte, Phys. Rev. Lett. **93**, 045003 (2004).
4. C. Li, Z. Zhang, and Z. Xu, Acta Opt. Sin. **16**, 299 (1996).
5. Q. Yang, A. Guo, X. Xie, L. Zhang, M. Sun, Q. Gao, M. Li, and Z. Lin, Chin. J. Lasers **35**, 1970 (2008).
6. M. Kalashnikov, A. Andreev, and H. Schönnagel, Proc. SPIE **7501**, 750104 (2009).
7. M. P. Kalashnikov, E. Risse, H. Schönnagel, and W. Sandner, Opt. Lett. **30**, 923 (2005).
8. N. Forget, A. Cotel, E. Brambrink, P. Audebert, C. Le Blanc, A. Jullien, and G. Chériaux, Opt. Lett. **30**, 2921 (2005).
9. J. Wang, P. Yuan, J. Ma, Y. Wang, G. Xie, and L. Qian, Opt. Express **21**, 15580 (2013).
10. C. Manzoni, J. Moses, F. X. Kärtner, and G. Cerullo, Opt. Express **19**, 8357 (2011).
11. A. Guo, H. Zhu, and Z. Yang, Acta Opt. Sin. **33**, 0214001 (2013).
12. Q. Liu, Z. Cen, and X. Li, Acta Opt. Sin. **33**, 0132001 (2013).
13. M. Yang, M. Zhong, and G. Ren, Acta Opt. Sin. **31**, 0507001 (2011).
14. V. Bagini, R. Borghi, F. Gori, A. M. Pacileo, M. Santarsiero, D. Ambrosini, and G. S. Spagnolo, J. Opt. Soc. Am. A **13**, 1385 (1996).
15. C. R. Wolfe and J. K. Lawson, Proc. SPIE **2633**, 361 (1995).
16. J. K. Lawson, J. M. Auerbach, and R. E. English, Jr., Proc. SPIE **3492**, 336 (1999).
17. Y. H. Chen, W. G. Zheng, W. J. Chen, S. B. He, J. Q. Su, Y. B. Chen, and J. Yuan, High Power Laser Part. Beams **17**, 403 (2005).
18. G. Xu, T. Wang, Z. Li, Y. Dai, Z. Lin, Y. Gu, and J. Zhu, Rev. Laser Eng. **36**, 1172 (2008).
19. Y. Wang, X. Ouyang, J. Ma, P. Yuan, G. Xu, and L. Qian, Chin. Phys. Lett. **30**, 024201 (2013).